Design and Fabrication of 90 GHz TES Polarimeter Detectors for the South Pole Telescope

V. Yefremenko, P. Ade, K. Aird, J. Austermann, J. Beall, D. Becker, B. Benson, L. Bleem, J. Britton, C. L. Chang, J. Carlstrom, H. Cho, T. de Haan, T. Crawford, A. Crites, A. Datesman, M. Dobbs, W. Everett, A. Ewall-Wice, E. George, N. Halverson, N. Harrington, J. Henning, G. Hilton, W. Holzapfel, S. Hoover, J. Hubmayr, K. Irwin, R. Keisler, J. Kennedy, A. Lee, E. Leitch, D. Li, M. Lueker, D. P. Marrone, J. McMahon, J. Mehl, S. Meyer, J. Montgomery, T. Montroy, T. Natoli, J. Nibarger, M. Niemack, V. Novosad, S. Padin, C. Pryke, C. Reichardt, J. Ruhl, B. Saliwanchik, J. Sayre, K. Schafer, E. Shirokoff, K. Story, K. Vanderlinde, J. Vieira, G. Wang, R. Williamson, K. W. Yoon, and E. Young

***Abstract*—We present information about the design and fabrication of 90 GHz Transition Edge Sensor (TES) detectors deployed in the SPTpol camera for investigation of the cosmic microwave background (CMB) polarization signal. The 90 GHz portion of the camera consists of 180 individual feedhorn modules with dual polarization-sensitive detectors. We discuss microfabrication details and the characterization of detector elements. Each detector incorporates a dipole-like Pd-Au absorber and Mo/Au TES thermometer, suspended together on a rectangular silicon nitride (SiN) membrane via 6 long (640 μm) and narrow (10 μm) legs. The geometry of the SiN legs was optimized to provide the target thermal conductance of 200 pW/K in combination with mechanical robustness and reliability. The proximity effect in superconductor (Mo) and normal metal (Au) bilayers was utilized to obtain a TES operating temperature between 520 and 540 mK. Excellent superconducting properties (transition width < 1 mK) and T_c uniformity (< 3 mK) across 2″ wafers were achieved by sputtering in a confocal system under a single vacuum using an independent RF bias applied to the substrate. Superconducting Nb dots patterned on the TES surface provided controllable broadening of the transition width. We report the results of transition measurements, along with characterization of film morphology.**

***Index Terms*—CMB polarimetry, low temperature detectors, PACS: 07.57.Kp, superconducting bolometer, transition edge sensor.**

Manuscript received October 8, 2012; accepted December 16, 2012. Date of publication December 24, 2012; date of current version January 25, 2013. The work at Argonne National Laboratory, including the use of facility at the Center for Nanoscale Materials, was supported by the Office of Science and Office of Basic Energy Sciences of the U.S. Department of Energy, under Contract DE-AC02-06CH11357. The work at the University of Chicago was supported by the National Science Foundation (NSF) under Grant ANT-0638937 and the NSF Physics Frontier Center Grant PHY-1125897. It also receives generous support from the Kavli Foundation and the Gordon and Betty Moore Foundation.

V. Yefremenko and G. Wang are with Argonne National Laboratory (ANL)-HEP Division, Argonne, IL 60439 USA (e-mail: yefremenko@anl.gov).

P. Ade is with Cardiff School of Physics and Astronomy, Cardiff University, UK.

K. Aird, B. Benson, L. Bleem, T. Crawford, A. Crites, W. Everett, A. Ewall-Wice, S. Hoover, R. Keisler, E. Leitch, J. Mehl, S. Meyer, J. Montgomery, T. Natoli, K. Story, and R. Williamson are with Kavli Institute for Cosmological Physics, Department of Physics, Enrico Fermi Institute, The University of Chicago, Chicago, IL 60637 USA.

J. Austermann, N. Halverson, and J. Henning are with the Department of Astrophysical and Planetary Sciences, University of Colorado, Boulder, CO 8030 USA.

J. Beall, D. Becker, J. Britton, H. Cho, G. Hilton, J. Hubmayr, K. Irwin, D. Li, J. Nibarger, and M. Niemack are with the National Institute of Science and Technology, Boulder, CO 80305 USA.

C. L. Chang and J. Carlstrom are with High Energy Physics Divison, Argonne National Laboratory, Argonne, IL 60439 USA and also with Kavli Institute for Cosmological Physics, Department of Physics, Enrico Fermi Institute, The University of Chicago, Chicago, IL 60637 USA.

T. de Haan, M. Dobbs, J. Kennedy, and K. Vanderlinde are with McGill University, Montreal H3A 0G4, QC, Canada.

A. Datesman and V. Novosad are with Materials Science Division, Argonne National Laboratory, Argonne, IL 60439 USA.

E. George, N. Harrington, W. Holzapfel, A. Lee, C. Reichardt, and E. Young are with the University of California, Berkeley, CA 94720 USA.

M. Lueker, S. Padin, E. Shirokoff, and J. Vieira are with the California Institute of Technology, Pasadena, CA 91125 USA.

D. P. Marrone is with Steward Observatory, University of Arizona, Tucson, AZ 85721 USA.

J. McMahon is with University of Michigan, Ann Arbor, MI, USA.

T. Montroy, J. Ruhl, B. Saliwanchik, and J. Sayre are with Case Western Reserve University, Cleveland, OH 44106 USA.

C. Pryke is with University of Minnesota, Minneapolis, MN 55455 USA.

K. Schafer is with the School of the Art Institute of Chicago, Chicago, IL 60603 USA.

K. W. Yoon is with Stanford University, Palo Alto, CA 94305 USA.

Color versions of one or more of the figures in this paper are available online at http://ieeexplore.ieee.org.

Digital Object Identifier 10.1109/TASC.2012.2235892

I. Introduction

ACCURATE measurement of the cosmic microwave background (CMB) polarization is a critical step in extending our knowledge both of the early Universe, and of fundamental physics at the highest energies.

Because current sub-mm/mm-wave bolometric arrays have already achieved background-limited performance, more sensitive measurements can be accomplished only by significantly increasing the number of detectors in a focal plane. A polarization-sensitive array incorporating 588 150 GHz and 180 90 GHz dual-polarization detectors designed for CMB observation was deployed on the South Pole Telescope (SPT) [1].

In this paper, we present details regarding the design and fabrication of the 90 GHz detectors. All pixels utilize Transition Edge Sensors (TES) as sensitive elements to provide measurement of the incident radiation. Design and technology efforts aimed to simultaneously achieve both the high sensitivity required for state-of-the-art measurement goals and the reproducibility and reliability needed for array deployment.

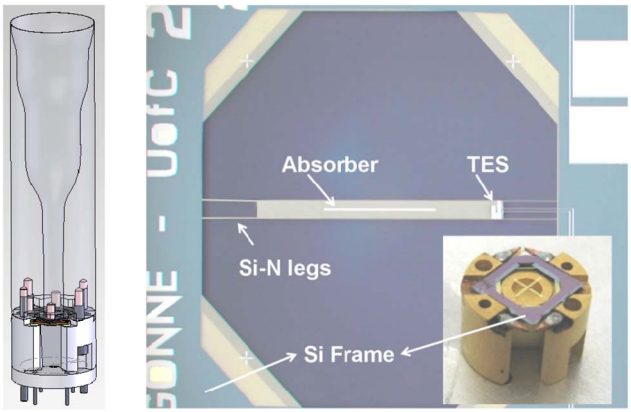

Fig. 1. Detector design. Geometry parameters of detector components are presented in Table I.

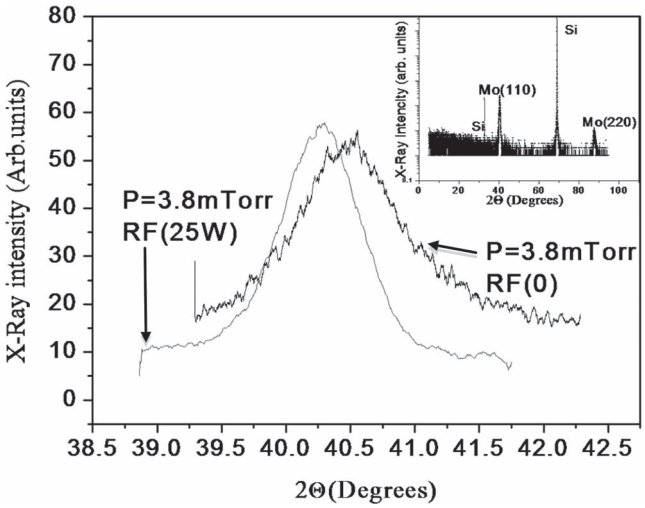

Fig. 2. XRD patterns of Mo films deposited with and without RF bias. The inset shows a full scan.

II. 90 GHz Pixel Design

The pixel design is shown in Fig. 1. A smoothwall profiled feedhorn and circular waveguide guide electromagnetic radiation from the telescope to the detector, where it is dissipated as heat in the dipole-like absorber. The detector design concept was successfully used in number of instruments [2]. The absorber and TES thermometer for temperature measurement are placed on a rectangular silicon nitride membrane suspended via 6 long and narrow legs. Thermal conductance between central island and the bath $(G_{\rm leg})$ was set by the geometry of the legs for target saturation power of 25 pW. The width of the membrane island was defined to provide $G_{\rm mem} \gg G_{\rm leg}$ and minimize temperature gradient between absorber and TES [3].

Each detector consists of two separate dies consisting of suspended membranes with silicon frames, carefully aligned perpendicularly and mounted face-to-face. The gap between the dies, which provides the required thermal and electrical isolation, is maintained using calibrated 25 μm wires bonded to metallized pads on the frames. Cross-shaped alignment markers located at interior corners of the frame enable accurate assembly. A corner etched away from each frame exposes the electrical connections on the facing die. The center frequency and bandwidth of the detector are determined by the filter stack, feedhorn, waveguide cutoff, backshort and geometry of the absorber.

III. Fabrication Details

A. Mo/Au Bilayer

The proximity effect in normal metal-superconductor bilayers is a popular approach to obtain target operating temperatures and sharp transition widths. Because Mo is insoluble with noble metals and Au is resistant to corrosion, we selected these materials for TES fabrication. The superconducting properties of Mo/Au bilayers have been analyzed in many laboratories [4]–[6]. The superconducting properties of Mo films, and the transparency of the S/N interface, are influenced strongly by the microfabrication process. This creates challenges for reproducibility and the long-term stability of detectors. We utilized RF biasing of the substrate during Mo deposition to improve film quality and keep the surface clean, creating an optimal interface with the normal metal layer.

The fabrication goals included a target operating temperature between 520 and 540 mK and high Tc uniformity across 2″ wafers. Both Mo and Au layers were deposited at room temperature under a single vacuum in a confocal DC magnetron sputtering system [7]. The base pressure of the system was about 3×10^{-8} Torr. Substrate holder rotation and adjustable-tilt sputtering guns (3″ diameter) provide high film thickness uniformity. In order to produce detectors with long-term stable properties, we optimized the residual stress of Mo films. Thin Mo films sputtered at room temperature typically exhibit a columnar structure with low density. Ion bombardment during film growth increases the density and changes the film stress from tensile to compressive. Light RF biasing of the substrate during deposition provided this bombardment. Varying deposition parameters including gun tilt, working pressure, and DC magnetron and RF bias power, we obtained slightly compressive (−50 Mpa) Mo films with thickness uniformity better than 0.5% over a diameter of 4″.

The structural features and morphological properties of Mo films sputtered with and without RF bias were analyzed using X-ray diffractometry (XRD) and atomic force microscopy (AFM). The X-ray diffraction measurements (shown in Fig. 2) indicate that Mo layers are polycrystalline, with a preferred orientation along the (110) crystal direction. The width (FWHM) of the peak decreases with additional substrate RF bias. This effect accords with increasing grain size and better strain uniformity.

The average Mo thin film grain size can be deduced from the width of the x-ray peaks using the Scherrer formula. The crystallite size was found to increase from ∼15 nm to ∼20 nm when RF power was applied to substrate.

AFM studies showed qualitative agreement with XRD measurements (Fig. 3): the films deposited without RF bias were rougher and possessed smaller grain size. The average RMS roughness decreased from 1.08 to 0.55 nm with RF bias applied.

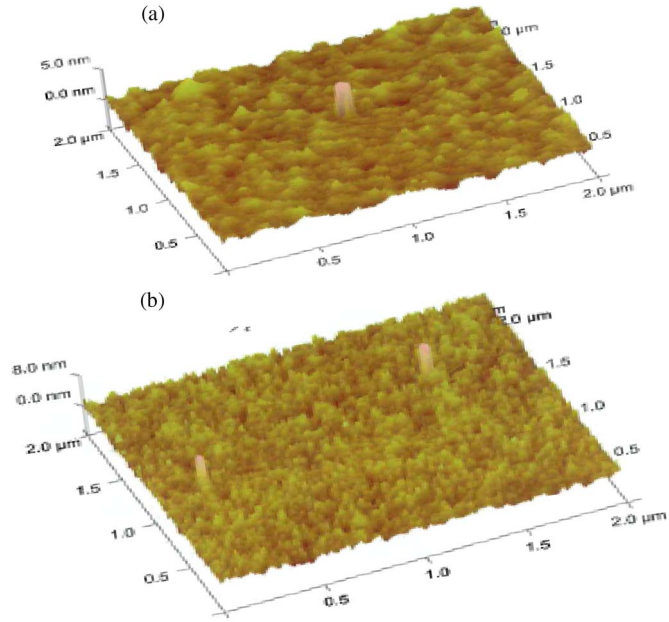

Fig. 3. AFM images of 23-nm-thick Mo films obtained with (a) and without (b) RF biasing.

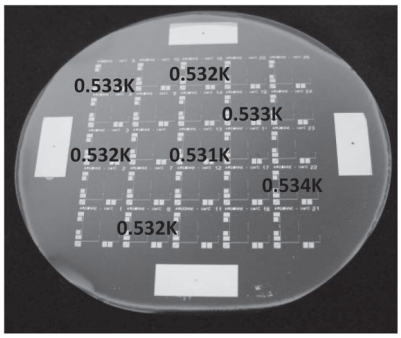

Fig. 4. Superconducting transition temperature uniformity over 2″ wafer. Transition width is less than 1 mK.

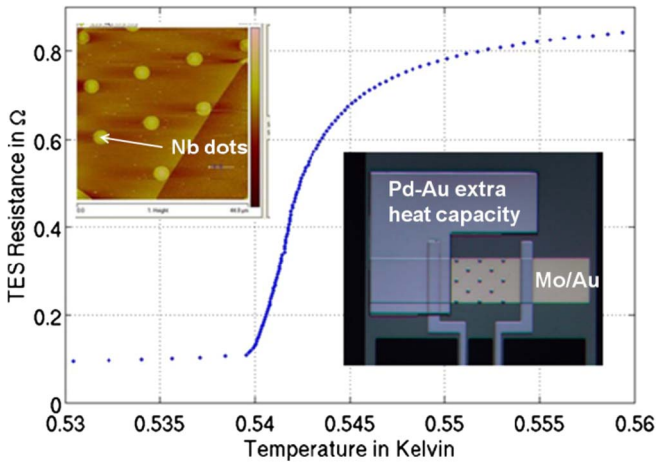

Fig. 5. Superconducting transition of modified TES. The inset shows TES design and AFM image of TES surface. The resistance of TES in operation points is about ∼0.7 Rn.

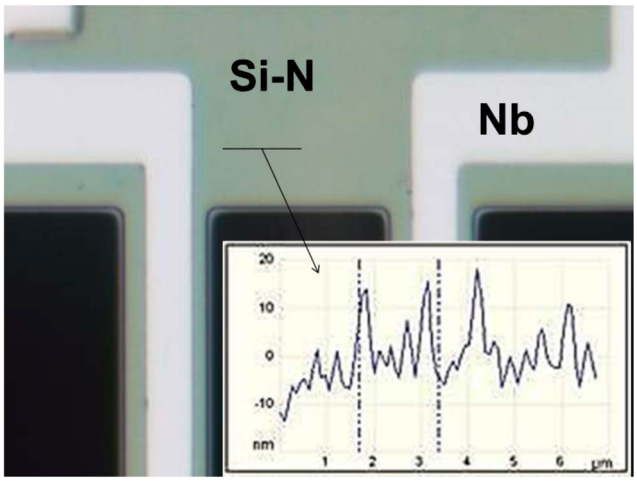

Fig. 6. Fragment of SiN legs and representative AFM scan of the membrane surface (inset). Root-mean square surface roughness ∼5.8 nm.

Due to the requirements of frequency-domain SQUID multiplexing, the resistance target is about $R_{\rm n} \sim 1\ \Omega$. Since the conductivity of gold is much higher than the normal state conductivity of Mo, the TES normal state resistance $R_{\rm n}$ is nearly a function of only the normal film thickness $d_{\rm n}$.

Based upon experiment, we found ∼30 nm Au to be an appropriate thickness for our design geometry. The proper thickness of the superconducting Mo layer was then determined based upon the target operating temperature of 530 mK. Deposition was performed under a single vacuum following RF cleaning of the substrate. Bilayers of 23 nm Mo and 30 nm Au exhibited very sharp $<$ 1 mK transitions with non-uniformity of Tc across the wafer $<$ 3 mK. The distribution of transition temperatures of TESs ($40\ \mu$m $\times$ $70\ \mu$m in size) lithographically patterned on a 2″ wafer is presented in Fig. 4.

B. Transition Edge Sensor

TES operation requires that thermal fluctuations be sufficiently damped out within the bandwidth of the electrical circuit. The analytical solution of two coupled differential equations describing the electrical and thermal circuits [8] shows that stable operation requires the electrical time constant to be less than the effective thermal time constant, including the effect of strong electro-thermal feedback. Based upon this understanding, we have altered our design (refer to Fig. 5) to increase the heat capacity and tailor the slope of the superconducting-normal transition. Palladium-gold alloy was utilized for the additional heat capacity because the material has good adhesion and a high specific heat at the operating temperature. Good thermal coupling between the TES and the Pd-Au layer was achieved by cleaning the contact area in oxygen and argon plasma.

Dots 3 μm in diameter and 120 nm thick made from superconducting Nb were patterned on the TES surface to controllably broaden the transition width. Due to proximity effect superconducting order parameter is enhanced in proximity to the Nb (dots), broadening the operating transition for stable performance. The effect of surface modification on the transition temperature and slope is presented in [9]. Additionally, the

TABLE I
DETECTOR COMPONENTS GEOMETRY AND FABRICATION PROCEDURES

Detector element	Material	Geometry	Fabrication process
TES	Mo(0.9996)/Au (0.9999) bilayer	Mo23nm/Au30nm , 40x70μm^2	Sputtering , 3.8mTorr , Mo - 267W+RF36W, 0.86A/sec, Au – 75W, 0.875A/sec Wet etching , K:I2(for Au) and H3PO4:HNO3:CH3COOH:H2O (for Mo)
Absorber	Pd-Au alloy	t=50nm, w=18μm, l=1328μm	Sputtering , 3mTorr, 75W, 0.9A/sec , Lift-off
Leads	Nb(0.9995)	t=120nm, w=5μm, l=700μm	Sputtering, 1.6mTorr,264W, 0.12A/sec, Lift-off
Dots	Nb(0.9995)	t=120nm, d=3μm	Sputtering, 1.6mTorr, 264W, 0.12A/s, Lift off
Extra Heat Capacity	Pd(40%)-Au(60%) alloy	t=450nm, area 12030μm^2	Sputtering, 3mTorr, 75W, 0.9A/sec , Lift-off
Bridges(legs)	SiN	t=1000nm, w=10μm, l=640μm	Back side Si wet KOH etching, top side RIE , CF4 160mTorr , 150W, 45sccm

Base pressure was 3-5x10^{-8}Torr , The highest temperature we used in fabrication procedure was 115C during 1 minute.

proximity effect with the Nb leads to the soft transition above T_c, (which provides limited responsivity under high loading conditions as expected when using ground-based calibration sources), and with the Pd-Au "bling" provides a finite normal resistance (which prevents the detector from latching in the superconducting state).

C. Absorber and Leads

Optical lithography and lift-off processes were used to fabricate both absorbers and leads. The TES leads consist of superconducting Nb 5 μm wide and 120 nm thick, with a total length between the sensor and the Si frame of 700 μm. The dipole-like absorber consists of a 50 nm thick layer of Pd-Au. Its $1162\ \mu\text{m} \times 18\ \mu\text{m}$ geometry was obtained using High-Frequency Structure Simulator (HFSS) to guarantee polarization sensitivity in the 95 GHz spectral range.

D. Thermal Link

Our devices were fabricated on amorphous low-stress Si-N films 1 μm thick grown by a commercial vendor on single crystal Si (100) double side polished 2″ wafers using low pressure chemical vapor deposition [10]. Patterning of the thermal link follows fabrication of the TES, absorber, and leads. The thickness of the wafers was $250 + -25\ \mu$m. Standard KOH wet etching of silicon (30% in water at 80 °C) was used to create a silicon nitride membrane window. The bridge structure was defined by reactive ion etching (RIE) with CF_4, followed by oxygen plasma cleaning. Before membrane perforation the reverse sides of the silicon nitride membranes were covered with a layer of sputtered aluminum 400 nm thick. The aluminum layer provides thermal sinking and mechanical support, and also improves plasma uniformity. After Si-N legs fabrication the Al film was removed from the bottom side of the membrane utilizing wet etching process.

A detailed study of the thermal properties of narrow beams of silicon nitride at low temperature was presented in [11].

The value of the thermal conductance depends very strongly upon the surface roughness, and therefore in turn upon the treatment of the silicon nitride material during fabrication. An AFM scan of the Si-N membrane of a completed detector is shown in Fig. 6. The Root Mean Square (RMS) value of the surface roughness of the Si-N layer before fabrication process was found to be approximately 0.3 nm. For two wafers we have studied after entire fabrication procedure the RMS of the roughness on the top surface exhibited 2.3 nm and 5.8 nm. The bottom side of the membrane had RMS about 1.9 nm for both devices. The roughness variation, the quality of released edges and inhomogeneities intrinsic to the membrane materials can be the reason of significant (up to 25%) variation of saturation power for detectors made from different wafers.

Fabrication process parameters and the geometry of detector components are summarized in Table I.

REFERENCES

[1] L. Bleem, P. Ade, K. Aird, J. Austermann, J. Beall, D. Becker, B. Benson, J. Britton, J. Carlstrom, C. L. Chang, H. Cho, T. de Haan, T. Crawford, A. Crites, A. Datesman, M. Dobbs, W. Everett, A. Ewall-Wice, E. George, N. Halverson, N. Harrington, J. Henning, G. Hilton, W. Holzapfel, S. Hoover, J. Hubmayr, K. Irwin, R. Keisler, J. Kennedy, A. Lee, E. Leitch, D. Li, M. Lueker, D. P. Marrone, J. McMahon, J. Mehl, S. Meyer, J. Montgomery, T. Montroy, T. Natoli, J. Nibarger, M. Niemack, V. Novosad, S. Padin, C. Pryke, C. Reichardt, J. Ruhl, B. Saliwanchik, J. Sayre, K. Schafer, E. Shirokoff, K. Story, K. Vanderlinde, J. Vieira, G. Wang, R. Williamson, V. Yefremenko, K. W. Yoon, and E. Young, "An overview of the SPTpol experiment," *J. Low Temp. Phys.*, vol. 167, pp. 859–864, Jun. 2012.

[2] W. C. Jones, R. S. Bhatia, J. J. Bock, and A. E. Lange, "A polariztion sensitive bolometric detector for observations of the cosmic microwave background," in *Proc. SPIE Int. Soc. Opt. Eng.*, 2003, vol. 4855, p. 227.

[3] G. Wang, V. Yefremenko, A. Datesman, V. Novosad, J. Pearson, G. Shustakova, R. Divan, J. Lee, C. L. Chang, J. McMahon, L. Bleem, A. T. Crites, T. Downes, J. Mehl, W. Everett, S. S. Meyer, J. E. Carlstrom, J. Sayer, and J. Ruhl, "Thermal modeling of absorber-coupled TES polarimeter," in *Proc. 13th Int. Workshop LTD AIP Conf.*, 2009, vol. 1185, pp. 334–337.

[4] R. Gonzalez-Arrabal, A. Camón, M. Parra-Borderías, L. Fabrega, J. Anguita, J. Sesé, and F. Briones, "Mo/Au bilayers deposited by sputtering at room temperature for transition edge sensor fabrication," *J. Low Temp. Phys.*, vol. 151, pp. 239–244, 2008.

[5] M. Yun, J. Bock, M. Keynon, C.-L. Kuo, H. G. Leduc, A. Turner, and M. J. Kim, "Fabrication of superconducting transition edge sensor based on Mo and Au bilayers," *Nucl. Instrum. Methods Phys. Res. A, Accel. Spectrom. Detect. Assoc. Equip.*, vol. 559, pp. 462–464, 2006.

[6] S. J. Smith, S. R. Bandler, A.-D. Brown, J. A. Chervenak, E. Figueroa-Feliciano, F. Finkbeiner, N. Iyomoto, R. L. Kelley, C. A. Kilbourne, F. S. Porter, and J. E. Sadleir, "Characterizing the superconducting-to-normal transition in Mo/Au transition-edge sensor bilayers," *J. Low Temp. Phys.*, vol. 151, pp. 195–200, 2008.

[7] AJA International ATC, 2000. [Online]. Available: http://www.ajaint.com/systems_atc.htm

[8] K. D. Irwin and G. C. Hilton, "Transition edge sensors," in *Chapter in Cryogenic Particle Detection*, vol. 99, *Topics in Applied Physics*, C. Enss, Ed. Berlin: Springer-Verlag, 2005, pp. 63–149.

[9] G. Wang, V. Yefremenko, C. L. Chang, V. Novosad, J. Pearson, R. Divan, and J. E. Carlstrom, "Mo/Au Bilayer Superconducting Transition Edge Sensor Tuning with Surface Modification Structures," submitted to ASC2012 Manuscript number 3EC-04.

[10] Rogue Valley Microelectronics. [Online]. Available: http://www.roguevalleymicro.com

[11] G. Wang, V. Yefremenko, V. Novosad, A. Datesman, J. Pearson, R. Divan, C. L. Chang, L. Bleem, A. T. Crites, J. Mehl, T. Natoli, J. McMahon, J. Sayre, J. Ruhl, S. S. Meyer, and J. E. Carlstrom, "Thermal properties of silicon nitride beams below one Kelvin," *IEEE Trans. Appl. Supercond.*, vol. 21, pp. 232–235, 2011.